ISBN: 978-3-95450-238-7 ISSN: 2226-0358 doi:10.18429/JACoW-ICALEPCS2023-M03A003

COMMISSIONING AND OPTIMIZATION OF THE SIRIUS FAST ORBIT FEEDBACK

D. O. Tavares*, M. S. Aguiar, F. H. Cardoso, E. P. Coelho, G. R. Cruz, F. H. de Sá, A. F. Giachero, L. Lin, S. R. Marques, A. C. S. Oliveira, G. S. Ramirez, E. N. Rolim†, L. M. Russo
Brazilian Synchrotron Light Laboratory (LNLS/CNPEM), Campinas, Brazil

Abstract

The SIRIUS fast orbit feedback (FOFB) system started operation for users in November 2022. The system design targeted an output disturbance rejection crossover frequency of 1 kHz by pursuing the minimization of loop delay. This paper gives an overview of the system architecture and technology choices, and reports on the commissioning, system identification and feedback loop optimization performed along the system's first year of operation.

INTRODUCTION

Figure 1 depicts the layout of the SIRIUS orbit feedback systems in one of the 20 sectors of the storage ring, showing the location of Beam Position Monitors (BPMs) and orbit corrector magnets.

A slow orbit feedback (SOFB) loop runs at an update rate of approximately 10 Hz to mitigate orbit drifts and errors caused by thermal effects, ground motion and residual misalignment. It comprises a set of 160 BPMs (320 beam position readings in total) as sensors and 281 actuators, more specifically, 120 horizontal and 160 vertical orbit corrector magnets plus the storage ring RF frequency.

The FOFB system, on the other hand, runs at an update rate of 48 kHz and is implemented upon a subset of 80 BPMs (160 beam position readings in total) and 80 dedicated fast orbit corrector magnets (160 corrector coils total)[1], targeting the rejection of fast and small amplitude orbit disturbances in the range of 0.1 Hz to 1 kHz, typically given by magnets vibration, magnets' power supply electrical ripple, injection transients and insertion devices movements. Despite being ready to include in the loop all the existing electron BPMs and beamline front-end XBPMs, the current configuration only includes electron BPMs adjacent to the light sources points.

DESIGN PRINCIPLES

The design of the SIRIUS FOFB system was driven by the minimization of the overall feedback loop delay. The main pursued design principles were:

1. Adopt the highest possible feedback loop update rate to decrease BPM decimation filters delay. Ideally, the loop rate should be high enough to make the data distribution network latency the dominant component of the delay budget.

2. Deploy high bandwidth actuators, providing an ideally flat frequency response above the closed loop sensitivity function crossover frequency.

3. Implement the real-time processing (FOFB feedback controller, data network and power supply's feedback loop) entirely in hardware (e.g., FPGAs) and make system integration as tight as possible to prevent unnecessary delays.

4. Use the minimum amount of sensors and actuators in the loop, just enough to provide exact correction at the light sources and avoid extra latency for data distribution.

Principle 1 has driven the selection of the BPMs electrode-switching frequency at a submultiple of the FOFB update rate. This makes the switching spurs lie exactly at the notches of the BPM Cascaded Integrator–Comb (CIC) decimation filters and gives a wide band for the decay of the decimation filter's frequency response, hence largely simplifying the filter's specification. Currently, the update rate is limited to 48 kHz (12 turns in the storage ring) due to the particular implementation of the data network in the FPGA, which does not allow pipelining multiple loop iterations, however there is no fundamental hardware limitation that prevents reaching higher rates in the future, for instance 96 kHz (6 turns).

Principle 2 drove the design of a thin 0.3 mm stainless steel vacuum chamber and low power linear amplifiers for the fast orbit correctors' power supply. A target bandwidth of 10 kHz (1 decade above the target crossover frequency) has been established. In combination with principle 3, the low power requirements led to the design of a compact fast corrector power supply in MicroTCA.4 Rear Transition Module (RTM) form factor. Its digital current regulation loops implemented in the same FPGA of the main FOFB controller. Therefore, the interface between the orbit feedback controller and the correctors' feeddback controller is nearly free of delay.

Principle 4 drove the separation of the slow and fast loops, in the same way other facilities have already adopted. It segments the requirements of high range low speed correctors and low range high speed correctors, greatly simplifying power supply design. The ammount of data to be exchanged in the FOFB network and its associated latency is also minimized.

* daniel.tavares@lnls.br
† erico.rolim@lnls.br

[1] The actual number of fast correctors included in the FOFB loop is currently 78 (156 coils). Two magnets of the injection straight section were temporarily repurposed to perform injection disturbance feed-forward with separate power supplies and control system.

ISBN: 978-3-95450-238-7 ISSN: 2226-0358 doi:10.18429/JACoW-ICALEPCS2023-M03A003

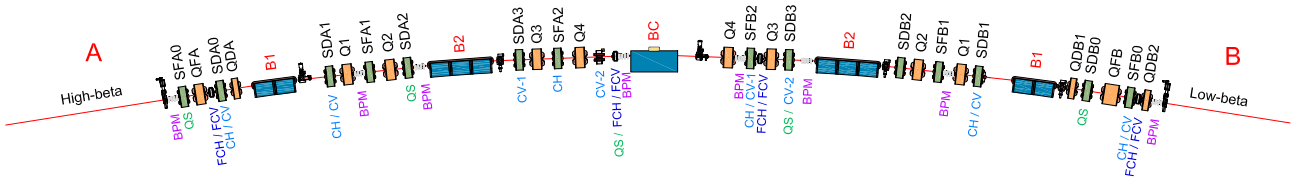

Figure 1: SIRIUS lattice showing FOFB corrector magnets (FCH / FCV) and SOFB corrector magnets (CH / CV). Only BPMs which are adjacent to straight sections and central bending magnets (BC) are included in the FOFB loop (4 per sector). All BPMs are included in the SOFB loop (8 per sector).

SYSTEM DESCRIPTION

The following sections detail the FOFB system architecture and chosen technologies.

Hardware Platform

The SIRIUS FOFB is based on the MicroTCA.4 hardware platform. Figure 2 shows one of the 20 MicroTCA.4 BPM and FOFB crates dedicated to process data from/to BPMs and fast orbit correctors of a single storage ring sector. The AMC FMC Carrier (AFC) [1], a general purpose processing card featuring an AMD/Xilinx Artix-7 FPGA, two FMC expansion slots, 2 GiB DRAM memory and support for Rear Transition Module boards (RTM), is used as base board for electron and photon BPM Digitizers, Timing Event Receiver and FOFB Controllers [2].

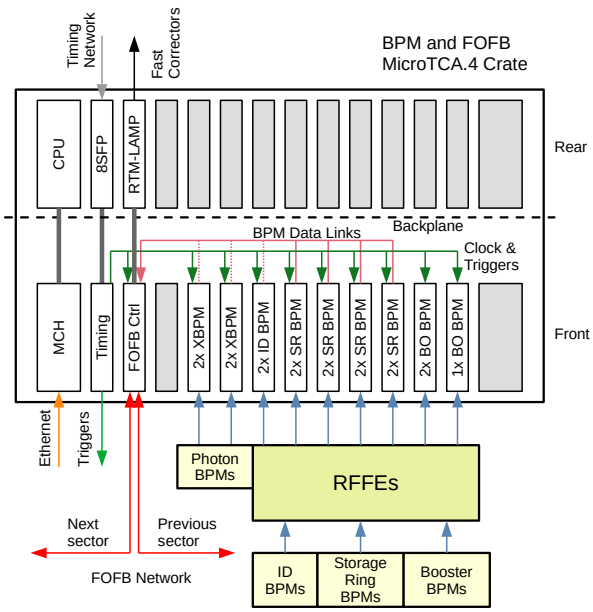

Figure 2: SIRIUS BPM and FOFB MicroTCA.4 crate layout.

The FOFB Controller consists of an AFC (v4.0.2), an RTM-LAMP and a CAENels 4SFP+ FMC card. Each Timing Event Receiver consists of an AFC (v3.1), an RTM 8 SFP+ and two FMC-5POF plastic fiber I/O. A BPM Digitizer consists of an AFC (v3.1) and up to two FMC ADC 4-channel 16-bit 250 MS/s cards.

BPM position data is received from the BPM Digitizers within the crate via multigigabit links routed through the backplane (customized full mesh interconnect) and distributed globally via a dedicated network (OM4 multimode optical fiber network physical medium) in bidirectional ring topology, connecting neighboring sectors' BPM and FOFB crates.

Sensors

The electron BPMs used in the FOFB loop are 24-mm-diameter circular BPMs employing bell-shaped button pickups [3,4]. The signals coming from the 4 buttons are filtered and amplified by the Radio Frequency Frontend (RFFE) electronics [5]. The RFFE is responsible of switching the RF channels of opposite BPM antennas at exactly 1/4 the FOFB update rate, i.e., 12 kHz, to mitigate static and dynamic channels imbalances mainly due to the components' thermal and intrinsic drifts. Long haul cables are not compensated. Digitization is performed by FMC ADC 250M cards [6] attached to the AFCv3.1 FPGA boards at MicroTCA.4 crates. The digital signal processing is based on the undersampling technique, using a sampling frequency of $382/h$, where $h = 864$ is SIRIUS's harmonic number. The digitized signals are digitally de-switched, down-converted and decimated with a simple 1 section 1 differential delay CIC filter to provide a stream of beam position readings at the FOFB rate. All major electronics modules were in-house developed or procured as open source/open hardware projects [2].

Beamline front-end X-ray BPMs (XBPMs) [4, 7] are also available to be included in the FOFB loop, but currently not used. They share the same digital platform and FPGA gateware design as the electron BPM Digitizers, differing only by the use of a commercial digitizer, CAENels FMC-PICO-1M4 [8].

Actuators

The 100 mm-long fast orbit corrector magnet has a FeSi core made of 0.5 mm laminations and 56-turn windings providing up to 30 µrad deflections on SIRIUS's 3 GeV electron beam. It combines both horizontal and vertical plane corrector coils into a single core and is placed around dedicated 0.3 mm-thick stainless steel vacuum chambers.

The magnets are driven by the RTM-LAMP power supply [9, 10], a MicroTCA.4 RTM board containing 12 channels capable of sourcing up to ±1 A currents. In the SIRIUS FOFB setting, only 8 channels are required, hence allowing a voltage swing of ±3.3 V, limited by the power envelope defined by the MicroTCA standard. Each channel consists

ISBN: 978-3-95450-238-7 ISSN: 2226-0358 doi:10.18429/JACoW-ICALEPCS2023-M03A003

essentially of a DAC, a Class AB power amplifier stage, a current sensing shunt resistor, an instrumentation amplifier and an ADC. The RTM-LAMP is controlled by the FOFB Controller board, sharing the same FPGA that is used to implement the FOFB control algorithm.

Real-time Processing

Figure 3 describes the main processing performed inside the FOFB Controller's FPGA and its data flow.

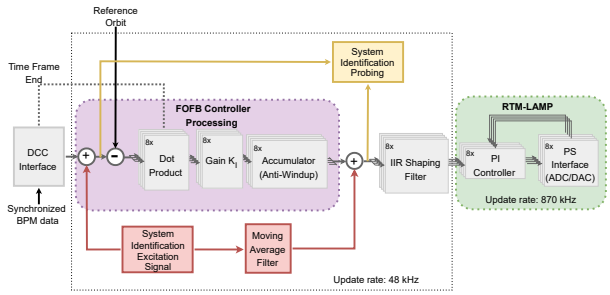

Figure 3: FOFB Controller real-time processing.

Network The Diamond Communication Controller (DCC) [11] is used as the layer 2 network protocol and deterministic packet forwarder to distribute the data from all BPMs included in the loop to all FOFB Controllers. A few modifications were made in the VHDL code to make it compatible with the SIRIUS interfaces [12, 13]. A configurable time slot (the *time frame*) is allotted to allow the complete propagation of data packets throughout the network. After this period has elapsed, the current setpoints are simultaneously updated in all power supplies controlled by the FOFB Controller. At SIRIUS the *time frame* is currently set up to 13.44 µs (2100 ticks of the multigigabit transceivers reference clock).

Control and System Identification The implementation of the control law, i.e. the calculation of fast correctors' current setpoints from the error orbit vector of a given loop iteration, was entirely written in VHDL and made available in [14]. The main blocks are: (i) dot product between the error orbit and each column of the correction matrix; (ii) integral controller, composed of a gain and accumulator with anti-windup; (iii) 10^{th}-order IIR filter with cascaded Second-Order Sections (SOS) in canonical form (direct form 2); and (iv) sum and multiplexing of data paths for injection and probing of excitation signals and waveforms for system identification purposes.

It is worth noting that the control law processing chains run in parallel and in stream mode, that is, the calculation of each orbit error from each received BPM data, and its multiplication by the corresponding correction matrix elements, is started as soon as the data is made available by the DCC, and follows immediately to be multiplied by the controller gain and accumulated, thus not accounting for additional delay.

Current Regulation Loop Despite running in the same FPGA as the FOFB processing, the fast corrector current regulation loops operate at a higher update rate, 870 kHz. Their dominant sources of delay are the ADC and DAC internal delays. The measured total delay is approximately 5 µs [9].

Software

The software responsible for controlling the fast orbit feedback system is composed of multiple layers and is fully integrated into EPICS. FOFB AFCs are controlled over PCIe by an EPICS IOC running on the MicroTCA.4 crates' CPUs [15, 16]. Unit conversions, high-level control and orchestration of the system is performed by multiple Python softIOCs [17]. Vectors with readback and monitor values from all power supplies are provided by a separate EPICS IOC [18].

Triggered acquisition of power supplies' waveforms (voltage, current setpoint and current reading) as well as synchronized orbit, control effort and probing signal waveforms for open loop and closed loop system identification are available, with upper bound of 1 million samples per channel.

CONTROL STRATEGY

The SIRIUS FOFB was designed having in mind that the plant dynamics can be dominated by the time delay only. Moreover, since the beam response itself can be fairly abstracted by an static response in synchrotrons like SIRIUS, where the betatron frequencies are of the order of 100 kHz), the MIMO behavior of the system can be decoupled by a typical pseudoinverse of the Orbit Response Matrix (ORM). The controller can then be reduced to a static decoupling matrix followed by multiple integral controllers.

Additional dynamics required to shape the loop response can be embedded in digital filters at the output of the FOFB controller. In other words, actuators' frequency response can then be equalized and pre-emphasized in order to compensate for uneven responses and/or to overcome bandwidth limitations of actuators and BPM electronics.

A conceptual description of the FOFB control loop system is illustrated in Fig. 4.

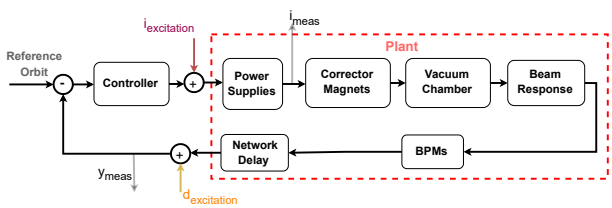

Figure 4: FOFB control loop model structure and system identification scheme.

Each block in the diagram represents a multiple-input multiple-output (MIMO) dynamic system and each arrow is used to designate a multidimensional signal of appropriate dimension. The Controller block consists of a purely

ISBN: 978-3-95450-238-7 ISSN: 2226-0358 doi:10.18429/JACoW-ICALEPCS2023-M03A003

integrative controller described by the following transfer matrix:

$$C_{\mathrm{F}}(z) = \left(K_{\mathrm{I}} \frac{T_s z}{z-1}\right) R_{\mathrm{F}}, \tag{1}$$

where K_{I} is the controller's integral gain, T_s stands for the sampling period of the control loop, and R_{F} is the orbit correction matrix. The R_{F} matrix can be obtained in two different ways: from the standard pseudoinverse of the measured orbit response matrix (ORM), M_{F}, or by considering the augmented matrix $(M_{\mathrm{F}}|\eta) = \left[\begin{array}{c|c} M_{\mathrm{F}} & \eta \end{array}\right]$, where the extra column η is the orbit response to a step variation on the storage ring RF frequency.

In the latter method, the last row of the pseudoinverse $(M_{\mathrm{F}}|\eta)^{+}$ is removed so that R_F has the appropriate dimensions for correction. This procedure for determining the correction matrix aims to spatially filter out orbit disturbance components which are caused by beam energy fluctuations and could only be appropriately corrected by acting on the RF frequency or phase. The SOFB system acts on the RF frequency to mitigate orbit distortions of this type which are caused by the slow variation of the storage ring circumference due to ground motion. The fast oscillations around the synchrotron tune (from 1 kHz to 2 kHz), on the other hand, are left free to occur without any counteraction from the FOFB loop. These oscillations do not deteriorate the beam stability at the beamline's light sources because all SIRIUS insertion devices are installed in dispersion-free straight sections and the high field dipole beamline source points have a very low dispersion function (~3 mm). On the other hand, this approach may interfere with the correction of distributed orbit distortion sources (e.g., bending magnets' electrical ripple, ramping Booster transients). The optimal solution depends on the actual beam disturbances.

Interoperation with SOFB

To deal with the DC currents that build up in the fast orbit corrector power supplies, a method to transfer the DC control effort to the SOFB running in parallel was implemented. Similar control architectures have already been carried out in other synchrotron facilities worldwide, and some of the challenges that emerge from the interaction between slow and fast orbit feedback correction systems as well as possible strategies to deal with them have already been reported in the accelerators community [19–23].

The scheme adopted at SIRIUS is inspired by the method described at [22], which proposes a periodic download of the DC components, that tend to accumulate at the fast correctors over time, into the slow ones. However, instead of downloading the full strength accumulated at the fast correctors all at once during each process iteration of the slow loop, only a fraction (currently 4 %) of the corrector kicks is transferred. In addition, differently from what is presented in [22], the reference orbit of the FOFB system is not updated, being kept constant and equal to the reference orbit of the SOFB system. The implemented scheme is described in Fig. 5.

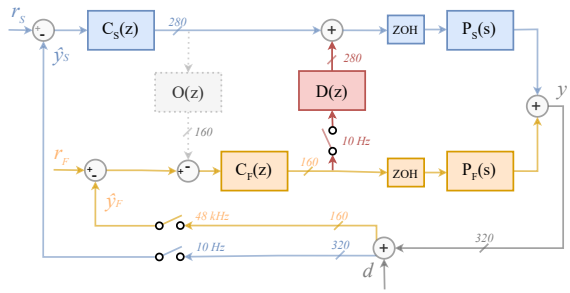

Figure 5: Feedback scheme for the concurrent operation of the slow and fast correction systems implemented at SIRIUS.

The blocks $C_{\mathrm{F}}(z)$ and $P_{\mathrm{F}}(s)$ indicate, respectively, the FOFB controller and the FOFB plant, which encompasses the dynamics of the FOFB power supplies, the fast corrector magnets, vacuum chamber, beam orbit response, BPM electronics (mainly decimation filters) and network delay. In a similar manner, the $C_{\mathrm{S}}(z)$ and $P_{\mathrm{S}}(s)$ blocks denote the SOFB controller and the SOFB plant.

The signal y in the diagram is used to designate the beam position along the storage ring (from which $\hat{y}_{\mathrm{F}}$ and $\hat{y}_{\mathrm{S}}$ are subspaces). d is the external orbit distortions. r_{F} and r_{S} are the reference orbit for each of the correction systems. It is worth noting that, even though it is possible to select the BPMs used in both loops independently, the systems are generally operated such that r_{F} is a subset of r_{S} and, consequently, that $\hat{y}_{\mathrm{F}}$ is a subspace of $\hat{y}_{\mathrm{S}}$.

The $D(z)$ block in Fig. 5, establishes the dynamics of the download process and can be represented by

$$D(z) = \left(f_{\mathrm{D}} \frac{z}{z-1}\right) M_{\mathrm{S}}^{+} M_{\mathrm{F}}^{c}, \tag{2}$$

where M_{F}^{c} is the complete FOFB ORM taking into account all BPMs that are included in the SOFB loop, M_{S}^{+} is the pseudoinverse of the SOFB ORM, and f_{D} stands for the fraction of the fast corrector strengths that are downloaded into the slow ones.

The download scheme is necessary for operation to avoid saturation of fast correctors. However, when operating with both loops closed and applying the strategy above, a residual DC orbit distortion of a few microns is observed on the BPMs that are included exclusively in the SOFB loop. This distortion is not spanned by the null space of the SOFB correction matrix and is directly related to the way the FOFB correction matrix is calculated. It only exists when the augmented matrix is used in the process. Further investigations are still under way.

Other FOFB-SOFB interoperation methods have been implemented and can be explored in the future, for instance the additional update of the FOFB reference orbit as described in [22] and denoted by the $O(z)$ block in Fig. 5. It is responsible for performing the prediction of the next orbit due to the SOFB actuation and transfer it as a part of the new reference to the FOFB system.

ISBN: 978-3-95450-238-7 ISSN: 2226-0358 doi:10.18429/JACoW-ICALEPCS2023-M03A003

COMMISSIONING AND OPERATION

The SIRIUS FOFB system was commissioned throughout October 2022 and entered operation in the following month. The operational experience so far revealed important limitations of the system as well as some unanticipated behaviors. Improvements and corrections were made along the first year of operation and some of them are reported in [24]. The following sections describe the most prominent findings and solutions.

Operation Improvements

During the course of its operation, a mechanism for synchronously opening the FOFB loop across all crates was proven to be needed. It prevents the FOFB from operating in scenarios of link losses or large orbit distortions.

Power Supply Issues

The design of the RTM-LAMP has met its requirements and has proven the general concept of employing low power linear amplifiers to drive FOFB actuators. However, a few implementation and reliability hurdles still remain. For instance, the ADC and DAC clocks are currently not synchronized to a multiple of the FOFB update rate, causing an uncertainty in the communication between FOFB Controller and the power supply of approximately 1.15 µs.

More importantly, 7 out of 160 power supply channels presented excessive noise levels whose sources have yet to be identified. One hypothesis is that the noise is coupled into the fast correctors' cables from an external source, since connecting the power supply channels to a local inductive load makes the noise disappear. In addition, 6 RTM-LAMP units have been replaced due to channel failure along one year of operation. The root cause has been identified as a soldering problem of the power amplifiers. A plan to re-solder the power amplifiers of all boards is currently in discussion.

Magnet Response Mismatch

SIRIUS fast corrector magnets were expected to have nearly identical dynamic responses in the band of interest (DC to 10 kHz) for magnets of the same type[2]. Moreover, the magnet admittance (voltage to current transfer function) was expected to be dominated by a single pole of an inductor-resistor (LR) circuit and the differences among correctors would arise from the spread of total series resistance (due to differences in cables' length) and the differences in inductance between the standard and rotated coil configurations. These two assumptions were proven wrong.

No dynamic response validation of all units — targeting the FOFB performance requirements — was specified by the FOFB team, resulting in a spread of dynamic responses among 18 magnets. The rigorous quality control in the manufacturing of the magnets covered only DC and low frequency characteristics. The fast corrector magnet validation was restricted to a single prototype [9].

Figure 6 shows the spread of the measured voltage-to-current frequency responses of a few magnets installed at SIRIUS (including long haul cables). It is worth noting that, at 1 kHz, the phase response of the unmatched correctors (from −60° to −70°) significantly differ from that of the matched ones (−80°). The measurements were performed by sweeping sine waves (voltage) with a signal generator and reading the voltage on a shunt resistor with an oscilloscope.

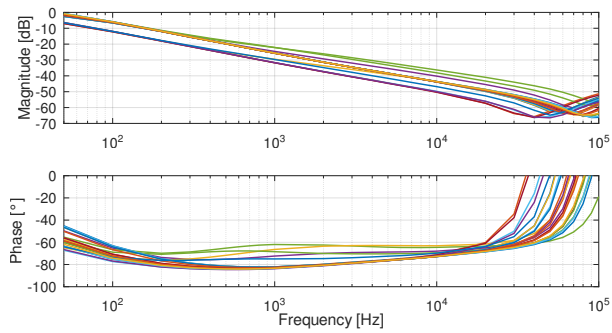

Figure 6: Fast correctors admittance in function of frequency (Sectors 02, 12 and 18).

Those divergent responses cannot be properly shaped by the PI controller implemented in the RTM-LAMP because the response does not have the first order expected of a purely LR circuit. There is a significant phase advance from 200 Hz to 10 kHz. Considering a frequency-dependent inductance model, the unmatched magnets' responses can alternatively be visualized as shown in Fig. 7. At lower frequencies, the inductance tends to the expected design values (around 6 mH for the rotated correctors and 3 mH for the standard ones). This discards the possibility of short-circuited windings. At 1 kHz some correctors deviate significantly from their nominal inductance. At frequencies higher than 30 kHz the capacitive effects of the cables start to dominate.

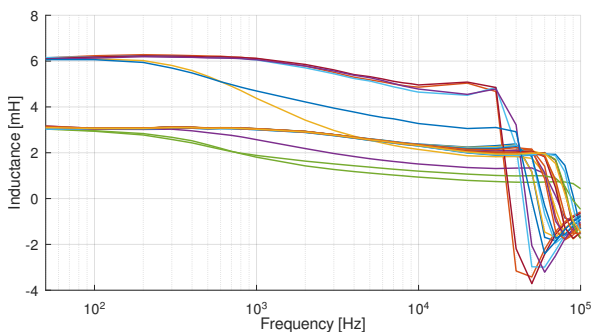

Figure 7: Fast correctors inductance over frequency (Sectors 02, 12 and 18).

The main hypothesis under consideration to explain these discrepancies is that some correctors have a partially short-circuited core, but disassembling the magnetic core to confirm this is not practical in the near term.

[2] There are two types of fast corrector magnets at SIRIUS storage ring: (i) "standard": coils at 0° and 90° orientations, 3 correctors per sector; (ii) "rotated": coils at 45° and −45° orientations, 1 corrector per sector.

ISBN: 978-3-95450-238-7 ISSN: 2226-0358 doi:10.18429/JACoW-ICALEPCS2023-M03A003

SYSTEM IDENTIFICATION AND PERFORMANCE EVALUATION

In order to provide estimates of the overall FOFB open loop dynamic response as well as the closed loop sensitivity function, a system identification feature was implemented in the FOFB Controller FPGA. As shown in Fig. 4, excitation signals can be injected either before the controller's actuator output ($i_{\text{excitation}}$, adding to fast correctors setpoints) or after the controller's sensor data input ($d_{\text{excitation}}$, adding to the orbit error), and the resulting system response can be read at the BPMs (y_{meas}) fast corrector current readings (i_{meas}).

The direction of the $i_{\text{excitation}}$ and $d_{\text{excitation}}$ excitation signals (*i.e.,* relative amplitude among all channels) can be arbitrarily set from the high level software, thus allowing excitation of specific corrector strength or orbit distortion profiles, one at a time, to probe specific spatial modes.

Currently, only Pseudorandom Binary Sequences (PRBS) are available as time signals. It is implemented as a Linear-Feedback Shift Register (LFSR) and allows the configuration of the sequence length ($N = 2^n - 1, n = 2, 3, 4, ..., 32$) and step duration (number of samples to be held for each value of the PRBS-generated sequence). A moving average filter with configurable length (from 1 to 8) is placed at the output of the PRBS generator to smooth signal edges that could saturate the voltage of the fast power supplies when high excitation amplitudes are used. PRBS has been chosen due to its simple implementation and broad spectrum excitation. The gateware design is modular and can be expanded in the future to include sine waves generators and arbitrary waveform loaded by software. Table 1 summarizes the chosen parameters for excitation signals for system identification.

The following sections describe the open loop and closed loop results obtained at SIRIUS.

Table 1: Excitation Signal Parameters

	Open Loop	Closed Loop
PRBS length (n)	127 (7)	511 (9)
PRBS step duration	3	4
Mov. Average length	2	N/A
Frequency grid step	126.5 Hz	23.6 Hz

Open Loop Identification

Open loop system identification was performed with PRBS signals to estimate the overall response (from current setpoint to beam position readings) for each fast orbit corrector. For each corrector system identification input signal a BPM reading is selected as output signal, more specifically the BPM with the largest response given by the FOFB ORM (M_{F}). The resulting identified transfer functions encompass power supply, magnet, vacuum chamber, beam (negligible) and BPM (mainly digital electronics) response, as well as the network delay.

From a total of 156 excited fast actuators, 133 FOFB open loop responses had very similar magnitude and phase. The remaining 23 responses have shown diverse magnitude and phase characteristics, due to the significant differences in magnets' admittances previously reported.

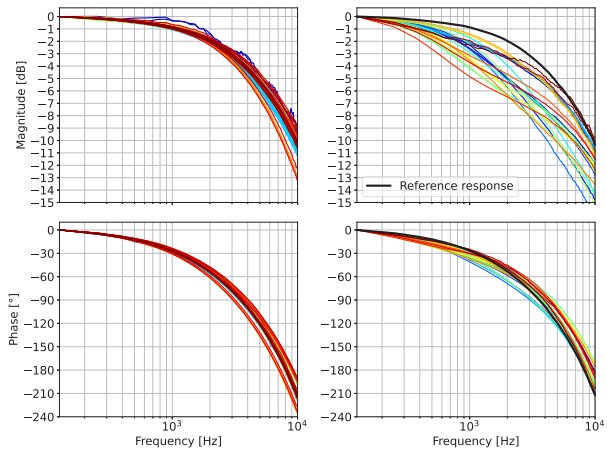

Figure 8: FOFB open loop frequency response corrector-by-corrector. Left: group of matched responses. Right: group of unmatched responses due to differences in magnet response. The reference response was arbitrarily selected as one of the matched correctors.

Closed Loop Identification

Closed loop system identification was performed with PRBS signals to estimate the FOFB output disturbance rejection transfer function, also known as the sensitivity function. The excitation was performed using the left-singular vectors of the FOFB augmented response matrix (i.e., columns of the matrix U in the singular value decomposition $(M_{\text{F}}|\eta) = USV^{\text{T}}$) one at a time in closed loop[3]. During the experiment, the FOFB loop was set with a correction matrix calculated from the augmented ORM.

Figure 9 shows the frequency responses to each excited orbit profile[4] when the FOFB controller's accumulator gain was set to $K_{\text{I}}T_{\text{S}} = 0.19$. A single-input-single-output (SISO) performance measurement was also performed employing the same controller gain but including only one BPM and one corrector in the loop. The SISO response serves as benchmark for the achievable performance when all actuators responses are well matched.

In the SISO case, the achieved crossover frequency is 1 kHz and the peak amplification is 5.5 dB at approximately 2 kHz.

The slight differences in the sensitivity function above 500 Hz across the several modes are believed to be caused by the actuator mismatch. Five modes do not follow the expected +20 dB/decade slope below 500 Hz because the RF

[3] Later analysis showed that exciting at the left-singular vectors of M_{F} instead of $(M_{\text{F}}|\eta)$ may have been preferred to minimize the excitation of non-intended modes.

[4] A complete mode-space analysis was not performed due to lack of time for data processing. It shall be reported in future publications.

ISBN: 978-3-95450-238-7 ISSN: 2226-0358 doi:10.18429/JACoW-ICALEPCS2023-M03A003

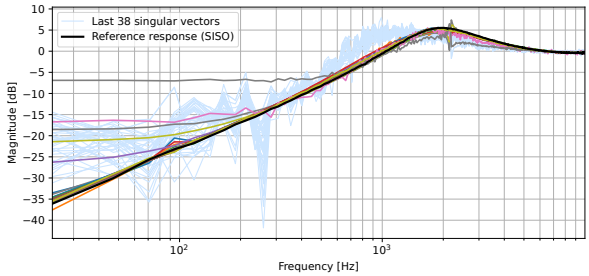

Figure 9: Disturbance rejection frequency responses per excited orbit profile. The response to the first 119 orbit profiles are plotted in colored traces. The remaining 38 responses are plotted in light blue and must be disregarded since their results are corrupted by actuators' saturation during the experiments. SISO performance is depicted as reference.

frequency/phase actuator is ignored to notch out orbit disturbances that can only be corrected by actuation in the longitudinal plane, and because 4 corrector coils (2 per plane) were temporarily removed from the loop. More complex behavior is seen above 2 kHz and is believed to be related to the longitudinal beam dynamics.

Achieved Orbit Stability

The overall effect of the FOFB system in the orbit stability is evaluated by integrating the Power Spectral Density (PSD) of the measured beam position data inside a frequency band and comparing it to the theoretical beam size for the cases when FOFB was disabled and enabled. Figure 10 summarizes the achieved orbit stability for two frequency bands (from 0.1 Hz to 100 Hz and from 0.1 Hz to 1 kHz). The achieved orbit stability in out-of-the-loop BPMs is better than 2 % in both planes.

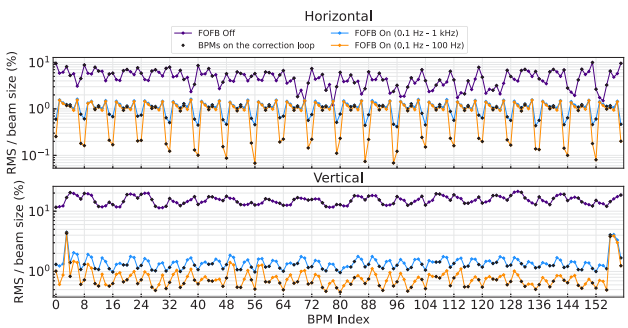

Figure 10: Orbit stability relative to beam size in all BPMs.

CONCLUSION

The one year operational experience with the SIRIUS FOFB system allowed the evolution of the system's reliability and performance. Diagnostics tools, interlocks and improvements in the user experience were implemented. Two system optimization campaigns were performed, in May and September 2023, and allowed the identification of bottlenecks and implementation issues that prevented increasing the loop gain. The developed embedded system identification tool was key to fully characterize the feedback loop and demonstrate its robustness to operate with high gains for user beam.

The target 1 kHz disturbance rejection crossover frequency has been achieved and provided orbit stability better than 2 % relative to beam size in both planes in out-of-the-loop BPMs. Despite the unexpected mismatch in actuator responses, the evaluated closed-loop responses analyzed so far agreed reasonably well with the SISO performance, used as proxy for achievable MIMO performance. A more rigorous mode-space analysis must be carried out to fully characterize the closed loop.

General improvements in the system's reliability and user experience for operation are foreseen. Major performance improvements are expected to come from the equalization of actuator responses and increase of loop update rate.

ACKNOWLEDGEMENTS

We would like to thank Gustavo Bruno for the main design choices and first prototype of the fast corrector power supply, Gabriel Brunheira for the review and abundant advice in the power supply design and system identification, and professor Ricardo Rodrigues (in memoriam) for his long standing support to the project and enthusiasm in pursuing the 1 kHz crossover frequency goal. We thank CNPEM's Magnets and Vacuum groups for the design of the fast corrector magnets and thin stainless steel vacuum chamber, as well as all the teams involved in the installation of BPMs, magnets, cabling, instrumentation racks and all other physical components. We express our gratitude to Günther Rehm, Sandira Gayadeen, Isa Uzun, James Rowland (in memoriam), Nicolas Hubert, Jean-Claude Denard, Boris Keil, Michael Böge, Eric Plouviez and Hans-Thomas Duhme for the countless discussions on orbit feedback loop optimization, slow and fast loops integration and system architecture. Their advice is the foundation of this work. We are grateful to Diamond Light Source for making the Diamond Communication Controller available for free use and modification. We give special thanks to our friend Sajjad Hussain Mirza (DESY) for the established collaboration in the last few years, actively participating in the FOFB machine studies during his visit to SIRIUS in May 2023 and engaging in insightful and in-depth discussions about orbit feedback systems with us. We also appreciate the interest of our other colleagues from DESY, Sven Pfeiffer and Holger Schlarb, in delving into the SIRIUS FOFB system for experience exchange and for their willingness to assist us with detailed magnet simulations in the near future.

REFERENCES

[1] AMC FMC Carrier PCB, https://ohwr.org/project/afc

[2] S.R. Marques, G.B.M. Bruno, L.M. Russo, H.A. Silva, and D.O. Tavares, "Commissioning of the Open Source Sirius BPM Electronics", in *Proc. IBIC'18*, Shanghai,

ISBN: 978-3-95450-238-7 ISSN: 2226-0358 doi:10.18429/JACoW-ICALEPCS2023-M03A003

China, Sep. 2018, pp. 196–203. doi:10.18429/JACoW-IBIC2018-TUOC03

[3] H.O.C. Duarte, S.R. Marques, and L. Sanfelici, "Design and Impedance Optimization of the SIRIUS BPM Button", in *Proc. IBIC'13*, Oxford, UK, Sep. 2013, paper TUPC07, pp. 365–368.

[4] H.O.C. Duarte, S.R. Marques, and D.O. Tavares, "Initial Experiences With Beam Diagnostics During Sirius Commissioning", presented at the IBIC'20, Santos, Brazil, Sep. 2020, paper MOAO02, unpublished.

[5] BPM RF Frontend PCBs, https://github.com/lnls-dig/rffe-hw

[6] 4-channel 16-bit 250 MS/s (700 MHz analog input bandwidth) ADC FMC PCB, https://ohwr.org/project/fmc-adc-250m-16b-4cha

[7] L.M. Volpe *et al.*, "High Heat Load Front Ends for Sirius", in *Proc. MEDSI'16*, Barcelona, Spain, Sep. 2016, pp. 324–326. doi:10.18429/JACoW-MEDSI2016-WEPE06

[8] 4-channel 20-bit 1 MSPS FMC Floating Ammeter, https://www.caenels.com/product/fmc-pico-1m4/

[9] A.F. Giachero, G.B.M. Bruno, L.M. Russo, and D.O. Tavares, "Fast Orbit Corrector Power Supply in MTCA.4 Form Factor for Sirius Light Source", in *Proc. IPAC'21*, Campinas, Brazil, May 2021, pp. 4307–4310. doi:10.18429/JACoW-IPAC2021-THPAB257

[10] RTM-LAMP PCB, https://github.com/lnls-dig/rtm-lamp-hw

[11] I.S. Uzun, R. Bartolini, G. Rehm, J.A. Dobbing, M.T. Heron, and J. Rowland, "Initial Design of the Fast Orbit Feedback System for DIAMOND Light Source", in *Proc. ICALEPCS'05*, Geneva, Switzerland, Oct. 2005, p. P3_030.

[12] Modified Sirius DCC Version, https://github.com/lnls-dig/CommsCtrlFPGA

[13] Original Diamond DCC Version, https://github.com/dls-controls/CommsCtrlFPGA

[14] FOFB Controller Gateware repository https://github.com/lnls-dig/fofb-ctrl-gw

[15] AFC IOC based on μHAL library, https://github.com/lnls-dig/afc-epics-ioc

[16] μHAL library, https://github.com/lnls-dig/uhal

[17] FOFB Python soft IOC, https://github.com/lnls-sirius/machine-applications

[18] FOFB monitor and readback vectors IOC, https://github.com/lnls-dig/fofb-mon

[19] J. Carwardine *et al.*, "APS Upgrade Integrated Beam Stability Experiments in the APS Storage Ring", presented at the IBIC'18, Shanghai, China, Sep. 2018, paper TUOC02, unpublished.

[20] E. Plouviez, L. Farvacque, J.M. Koch, J.L. Pons, and F. Uberto, "Improvement of the Fast Orbit Correction on the ESRF Storage Ring", in *Proc. DIPAC'09*, Basel, Switzerland, May 2009, paper TUPD05, pp. 297–299.

[21] P.C. Chiu, K.T. Hsu, K.H. Hu, C.H. Kuo, and C.Y. Wu, "Fast Orbit Feedback Scheme and Implementation for Taiwan Photon Source", in *Proc. IPAC'13*, Shanghai, China, May 2013, paper TUOCB202, pp. 1146–1148.

[22] N. Hubert, L. Cassinari, J. Denard, A. Nadji, and L. S. Nadolski, "Global Fast Orbit Feedback System Down to DC using Fast and Slow Correctors", in *Proc. DIPAC'09*, Basel, Switzerland, May 2009, paper MOOC01, pp. 27–31

[23] C. Steier, E.E. Domning, T. Scarvie, and E. Williams, "Operational Experience Integrating Slow and Fast Orbit Feedbacks at the ALS", in *Proc. EPAC'04*, Lucerne, Switzerland, Jul. 2004, paper THPLT141, pp. 2786–2788.

[24] L. Liu *et al.*, "Status of SIRIUS operation with users", in *Proc. IPAC'23*, Venice, Italy, May 2023, pp. 2586-2589. doi:10.18429/JACoW-IPAC2023-WEOGA2

[25] D.O. Tavares and S.R. Marques, "Performance Optimization for the LNLS Fast Orbit Feedback System", in *Proc. PAC'11*, New York, NY, USA, Mar.-Apr. 2011, paper WEODN3, pp. 1485–1487.

[26] L.-H. Yu, S. Krinsky, O. Singh, and F.J. Willeke, "The Performance of a Fast Closed Orbit Feedback System with Combined Fast and Slow Correctors", in *Proc. EPAC'08*, Genoa, Italy, Jun. 2008, paper THPC140, pp. 3315–3317.